Available online at www.sciencedirect.com
SCIENCE DIRECT®
Electrochimica Acta 50 (2005) 1931–1937
ELECTROCHIMICA Acta
www.elsevier.com/locate/electacta

Low temperature performance of copper/nickel modified $LiMn_2O_4$ spinels

Y. Ein-Eli[a,*], R.C. Urian[b,1], W. Wen[b], S. Mukerjee[b,**]

[a] *Department of Materials Engineering, Technion-Israel Institute of Technology, Technion City, Haifa 32000, Israel*
[b] *Department of Chemistry and Chemical Biology, Northeastern University, 360 Huntington Avenue, Boston, MA 02115, USA*

Received 2 August 2004; received in revised form 2 September 2004; accepted 3 September 2004
Available online 14 November 2004

Abstract

This study presents an evaluation of structural changes resulting from cycling modified copper/nickel $LiMn_2O_4$ spinels at 263 K. In situ synchrotron XRD shows that cycling $LiMn_2O_4$ at 263 K resulted in the formation of mixed cubic and tetragonal phases with a consequent lower capacity. The differential capacitance profile normally exhibiting two peaks at 298 K is modified, showing only one oxidation peak at 263 K in the 4 V region. The changes observed are attributed to interactions between Jahn–Teller active Mn^{3+} species and Li^+ ions. These changes are not observed once copper/nickel modified spinels are being evaluated, because of the decrease in Mn^{3+} population. All the observed changes are fully reversible once the material is cycled back at 298 K.

Keywords: Cu–Ni modified Mn spinels; Low temperature behavior; In situ XRD; Structural modifications

1. Introduction

$LiMn_2O_4$ has been considered until recently as a leading candidate for the next generation of materials for rechargeable batteries. The material is inexpensive compared to lithiated cobalt and nickel oxides and it is considered as environmentally friendly. However, $LiMn_2O_4$ does have its own set of disadvantages, severely preventing its implementation as a commercial material in Li-ion cells. Of a special interest are those associated with capacity fading in the 4 V region. These problems are associated with:

(i) loss of oxygen in the delithiated state [1–5].
(ii) high solubility of the spinel material as a result of acid attack followed by a disproportionate reaction [$2Mn^{3+}_{(solid)} \rightarrow Mn^{4+}_{(solid)} + Mn^{2+}_{(solution)}$].
(iii) average oxidation state of the manganese is 3.5 and thus, any small perturbation influencing the oxidation state may alter the ratio of low spin Mn^{4+} ($t^3_{2g} - e_{2g}$) and Jahn–Teller (JT) active high spin Mn^{3+} ($t^3_{2g} - e^1_{2g}$) state. The material is thus susceptible to structural distortions and fatigue due to the onset of cooperative JT distortion, which can lead to severe capacity fading. Jahn–Teller distortion can be induced by either insertion of a second lithium ion or by a decrease in temperature.

Low temperature-induced JT distortion is a result of the formation of discrete energy levels due to a lack of polaron hoping of the e_g electrons between Mn^{4+} and Mn^{3+} [6]. This results in a distortion of the 90° Mn–O–Mn bonds and the loss of t_{2g} and e_g orbital overlaps with mutually orthogonal oxygen 2p orbitals. This phenomenon has been reported to occur just below room temperature in the range of 280–290 K with a 10–13° hysteresis [1].

Unlike the temperature-induced effect, JT distortion via intercalation of excess lithium ion into the spinel structure results in a surface enhancement of the Mn^{3+}/Mn^{4+} ratio [7]. This mechanism propagates from the surface into the bulk of the material, with concomitant structural stress and

* Corresponding author. Tel.: +972 4 829 4588x5677; fax: +972 4 829 4588x5677.
** Co-corresponding author. Tel.: +1 617 373 8949; fax: +1 617 373 8949.
E-mail addresses: eineli@tx.technion.ac.il (Y. Ein-Eli), s.mukerjee@neu.edu (S. Mukerjee).
[1] Present address: Integrated Fuel Cell Technologies Inc., Burlington, MA, USA.

0013-4686/$ – see front matter © 2004 Elsevier Ltd. All rights reserved.
doi:10.1016/j.electacta.2004.09.002

fracture domains, which results in continued capacity fading. The Mn^{3+}-rich regions are subject to dissolution and the resulting phase boundary separation between cubic and tetragonal regions can all contribute to a rapid capacity fading [7].

A systematic investigation of the low temperatures effect on the structural distortion of $LiMn_2O_4$ has been reported by Yamada and Tanaka [1], who observed a cubic to tetragonal distortion in which the material had a volume fraction of 35% cubic and 65% tetragonal at 260 K. Subsequent to this study, Rousse [2] reported on a phase transition from cubic to a purely orthorhombic with columnar charge ordering over five different crystallographic sites. Additional work has focused on electric and magnetic properties [3,4] of the spinel at low temperature. Very little work has been published on the correlation between low temperatures induced distortions and cell performance. Some researchers have postulated that no change in the performance should occur [1], while others have suggested a change in lithium ion's transfer mechanism [5]. Several groups have reported on cells performance at 273 K utilizing $LiMn_2O_4$ [8,9]. These studies reported insignificant changes in the recorded capacity, compared with room temperature data.

Prior investigations [10–12] on electrochemical behavior of $LiCu_{0.5}Mn_{1.5}O_4$ indicated that once this material is charged, Mn(III) is oxidized to Mn(IV) at the lower potential region (3.9–4.5 V) and the lattice contracts as Li ions are removed from the lattice. This novel material also possesses a reversible ultra high potential activity at 5 V. At the upper potential plateau (4.8–5 V) no further changes in the Mn oxidation state occur, while Cu(II) is oxidized to Cu(III) without any further contraction of the lattice [11,12]. While the oxidation of Mn observed at the lower potential plateau (3.9–4.5 V) modifies the coordination symmetry around the copper, the concomitant oxidation of Cu at ultra high potentials (4.8–5 V), causes a similar modification of coordination symmetry around the Mn [12]. These processes are reversible and occur while maintaining a single cubic spinel phase.

More extensive works conducted by our groups showed that Li can be extracted at ambient temperature from copper/nickel modified Mn spinels structures (with the general formulation of $LiNi_xCu_{0.5-x}Mn_{1.5}O_4$, where $x = 0$, 0.25 and 0.5) in two potential regions: 3.3–4.5 and 4.6–5.1 V [13,14]. The upper potential plateau is dependent on the value of x; that is, as the Ni content increases, the potential plateau decreases from 4.95 to 4.6 V. At the same time, the reversible capacity increases from approximately 72 mAh/g ($x = 0$) to 120 mAh/g ($x = 0.5$). In situ XAS spectroscopy shows that for a Cu-rich composition ($x = 0$), the two potential plateaus correspond to change in Mn oxidation state from 3.7 to 4.0 and a change in Cu oxidation state from 2.18 to 2.84 [14]. For $LiCu_{0.25}Ni_{0.25}Mn_{1.5}O_4$ (composition with $x = 0.25$) the change in Mn oxidation state is smaller (from 3.8 to 4.0). Thus, most of the recorded capacity is originated from changes in Ni oxidation state (from 1.98 to 3.47) and to a lesser extent from Cu oxidation state modification (from 2.14 to 2.43). The measured capacity obtained from discharging the material with a composition of $x = 0.5$ ($LiNi_{0.5}Mn_{1.5}O_4$) is primarily originated from a change in the Ni oxidation state (from 2.2 to 3.8).

In situ XRD measurements performed in the 4–5 V region show a single-phase transition during charge and discharge of Cu-rich compound ($LiCu_{0.5}Mn_{1.5}O_4$, $x = 0.0$) [12]. This is in contrast to two and three phases coexistence in the compositions containing $x = 0.25$ and 0.5 ($LiCu_{0.25}Ni_{0.25}Mn_{1.5}O_4$ and $LiNi_{0.5}Mn_{1.5}O_4$, respectively) [13,14]. This may explain the superior cycle life behavior of the Cu-rich sample ($x = 0$) in this ultra-high potential region at ambient temperature [10–12]. In contrast to this unique behavior, the Cu-rich sample shows the onset of JT distortions in the 3 V region. Such distortions are absent in Ni substituted spinel samples ($x = 0.25$ and 0.5) [14].

The main objective of this research is to study the electrochemical behavior of manganese oxide spinels at low temperatures and to correlate this behavior with structural transformations occurring due to the temperature modification (from 298 to 263 K). This is motivated by an attempt to understand the effect of structural transformations induced by transition to low temperatures as opposed to those resulting from intercalation of a second Li into the spinel structure. As a part of this study, modified Cu and Ni manganese oxide spinels were used as model structures to enable a better understanding of the low temperature induced structural changes. The choice of Cu- and Ni-doped spinels was predicated by the wealth of prior data at ambient temperature. As mentioned earlier, these modified spinels exhibit unique structural and electrochemical characteristics, having the potential to serve as probes for better understanding low temperature behavior.

2. Experimental

Commercially available $LiMn_2O_4$ with excess Li (1.02) and battery electrolyte (EC:DMC = 1:1, v/v, 1 M $LiPF_6$) were obtained from EM Merck. $LiCu_{0.5}Mn_{1.5}O_4$ and $LiNi_{0.5}Mn_{1.5}O_4$ were prepared according to methodology described elsewhere [10–13]. The spectro-electrochemical cell and electrodes constructions are described in references [12–18]. Li foil was used as both anode and reference electrodes, while the working electrode had a composition of 80% active material, 10% Shawinigan Acetylene Black and 10% Kynar PVDF (Autochem, France). Electrochemical data (differential capacitance, charge and discharge profiles) were acquired using a battery cycler (Arbin MSTAT system and software, Arbin Instruments, Texas). Electrochemical data were measured in the same spectro-electrochemical cells as used in collecting in situ synchrotron based XRD and XAS measurements [17]. Rates of $C/10$ (current density of 100 $\mu A/cm^2$) were applied in cell galvanostatic measurements with cut-off potentials of 3.3 and 4.5 V for the un-doped manganese oxide spinel. Charge cut-off potential of 5.2 V was applied for the

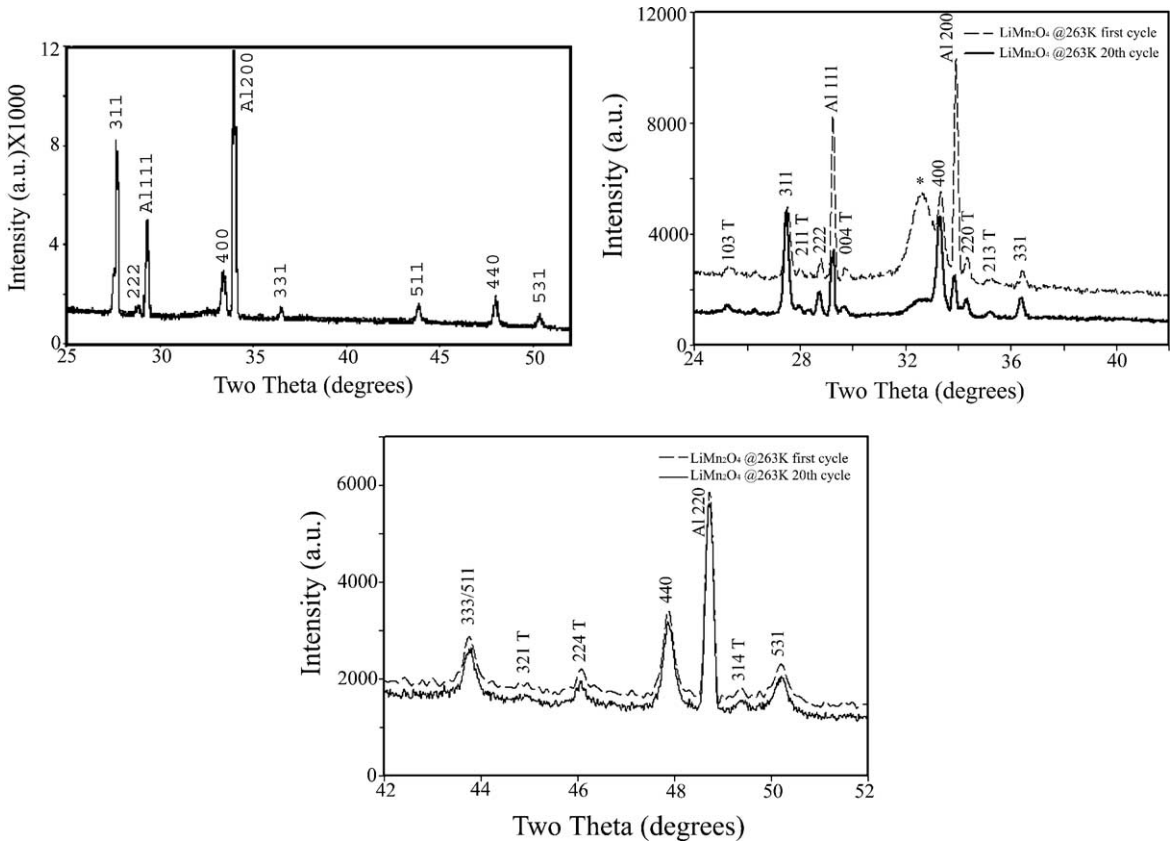

Fig. 1. (a) XRD diffraction patterns of $LiMn_2O_4$ cycled at 298 K showing the expected cubic phase. (b) Diffraction patterns of $LiMn_2O_4$ cycled at 263 K (data presented between 2 theta angle of 22 and 42) and (c) Diffraction patterns of $LiMn_2O_4$ cycled at 263 K (data presented between 2 theta angle of 42 and 52), showing both cubic and the tetragonal phases.

Cu- and Ni-doped spinels. The lower cut-off potential was also set to 3.3 V for the lower operating temperatures in order to ensure that any observed JT distortion is not due to intercalation of a second lithium ion extraction.

In situ XRD measurements were performed in a transmission mode [17] using X-18A beam line at National Synchrotron Light Source (NSLS) at Brookhaven National Laboratory (BNL) with a wavelength of 1.195 Å. Low temperature experiments and measurements, including in situ spectroscopy, were performed using a home-made chiller apparatus. This set-up allows the performance of low temperature in situ synchrotron XRD and XAS measurements in a set temperature within $\pm 1\,^{\circ}C$ precision. Additional spectra of the materials were taken at the beginning and the end of charge cycles, following a 30-min relaxation period. The acquisition time for each spectrum was 30 min. In addition to in situ XRD measurements, in situ XAS measurements were also performed in a transmission mode at the synchrotron light source (NSLS) at BNL using beam line X11-A. Details of the monochromator set up, resolution, and optics of the beam line are discussed in details elsewhere [13,14]. The prime motivation for XAS measurements was to use the near edge part of the spectra (X-ray Absorption Near Edge Structure, XANES) to determine the oxidation state of manganese in the mixed metal cathode materials. Nominal energy resolution at 9 keV (Cu K edge) was ± 1.1 eV. Valance state measurements by XANES reflect the difference in energy of an initially unexcited atom in the solid and the same atoms with a core hole plus a photoelectron in the lowest energy unoccupied state of appropriate symmetry as determined by dipole selection rules. Oxidation state changes were based on standard curves obtained from shift in the XANES spectra at the Mn K edge using standard compounds. Details of this measurement, including shifts of XANES per oxidation state change are giving elsewhere [12–18]. Manganese oxidation states were measured with the use of several standards which include Mn, MnO, Mn_2O_3, MnO_2 (CMD, chemically manganese dioxide and EMD, electrolytic manganese dioxide).

3. Result and discussion

3.1. XRD studies

Fig. 1 presents in situ XRD patterns obtained from $LiMn_2O_4$ in a fully discharged state, measured subsequent to 20 cycles at 298 K (Fig. 1a) and 263 K (Fig. 1b and c). XRD pattern of $LiMn_2O_4$ cycled at 263 K obtained between 2 theta angle of 22 and 42 is presented in Fig. 1b, while data obtained between 2 theta angle of 42 and 52 is presented in

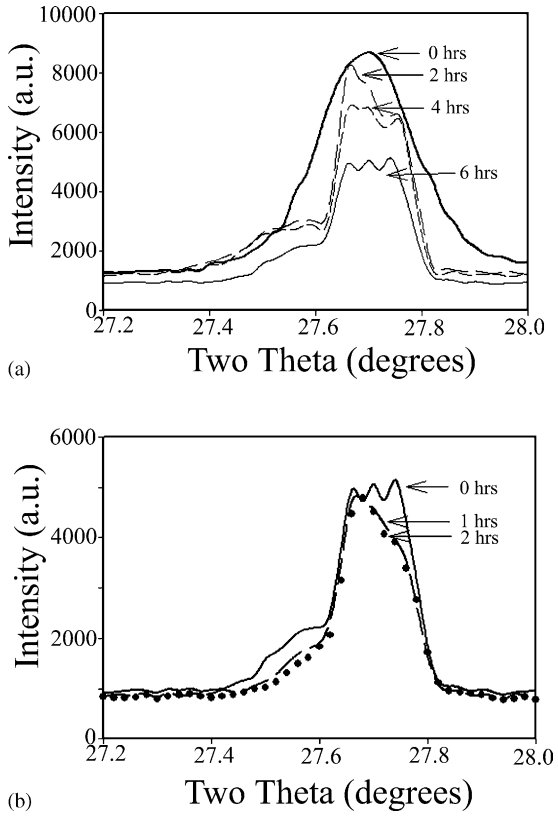

Fig. 2. (a) Magnification of the 3 1 1 peak, showing the evolution of the triplet splitting from its single peak at room temperature to its small triplet split peaks after 10 h at 263 K. (b) Magnification of the 3 1 1 peak showing the reversion of orthorhombic distortion back to a cubic phase.

Fig. 1c. No changes in the spinel electrode diffraction patterns were observed in the first 20 cycles at 298 K. The expected diffraction pattern of the sample cycled at 298 K is of a cubic lattice structure, where oxygen anions occupy 32e sites, manganese cations occupy the octahedral 16d sites and lithium ions occupy the tetrahedral 8a sites. However, the diffraction pattern obtained from spinel electrode cycled at 263 K represents a mixture of both cubic and tetragonal phases. This is represented by an expanded view of the diffraction pattern in Fig. 1b and c, where the appropriate diffraction lines are marked.

Prior data [1,19–21] on low temperature diffraction pattern of $LiMn_2O_4$ has focused on bulk powder properties and not on low temperature cycled electrodes. Yamada and Tanaka [1], who demonstrated a cubic → tetragonal distortion with a mixture of the two phases, showed a triplet splitting of the (4 4 0) peak, which is not observed in our studies. Pristine $LiMn_2O_4$ electrode immersed in the electrolyte for 6 h, without any electrochemical cycling did not show a (4 4 0) peak triplet splitting. We also did not observe such a change in the diffraction patterns obtained from low temperature cycling (Fig. 1b and c). The only structural change that was observed albeit after 6 h of immersion (without electrochemical cycling) was a small triplet splitting of the (3 1 1) peak (Fig. 2a). This type of peak splitting has been reported by Rousse et al. [9], who have ascribed it to a cubic → orthorhombic transition. However, in a contrast to this prior report [9], no splitting of the (4 0 0) peak nor emergence of low intensity super lattice diffraction lines were found, even after 6 h of immersion. The reason for the lack of a distinctive phase transformation and the length of time it did take to observe a single peak distortion can be attributed to the lithium rich spinel used in this study. According to Yamada [22], substitution of lithium into 16d sites would result in an increase of the oxidation state of the manganese and thus the transition temperature is reduced and a decreased amount of distortion is observed. A distortion would no longer be observed once $x = 0.033$ for $Li(Li_xMn_{2-x})O_4$ [22]. This behavior was found to be reversible as shown in Fig. 2b, where the peak splitting slowly disappeared to revert to a single peak associated with a temperature raise from 263 to 298 K.

3.2. Electrochemical evaluation

Our objectives in studying low temperature behavior of lithiated manganese spinels were primarily focused on the effect of Mn^{3+}/Mn^{4+} ratio in the manganese oxide spinel matrix. Therefore, cycling and differential capacitance measurements of two model compounds were performed. $LiCu_{0.5}Mn_{1.5}O_4$ and $LiNi_{0.5}Mn_{1.5}O_4$ as cathode electrode materials were evaluated at 298 and 263 K. The addition of a second divalent metal into the spinel matrix increases the oxidation state of the manganese as shown in Fig. 3. In the Cu-doped manganese oxide spinels the one electron reaction of $Cu^{+2} \rightarrow Cu^{+3}$ in $LiCu_{0.5}Mn_{1.5}O_4$ occurs at a potential of 4.95 V, while in the case of a Ni-doped sample, the two electron reaction of Ni^{+2} to Ni^{+4} [23,24] takes place 'only' at a potential of 4.6 V. The inclusion of Ni into Mn oxide spinel reduces the capacity obtained in the low-potential plateau (3.3–4.5 V). However, this capacity, related to the reversible reaction of $Mn^{+3} \rightarrow Mn^{+4}$ is not totally eliminated since not all of the Mn ions in the spinel matrix are at the +4 oxidation state, but rather exhibit an average oxidation state +3.87 (Fig. 3). The manganese oxidation state in the copper rich manganese oxide spinel is shown to be approximately +3.75.

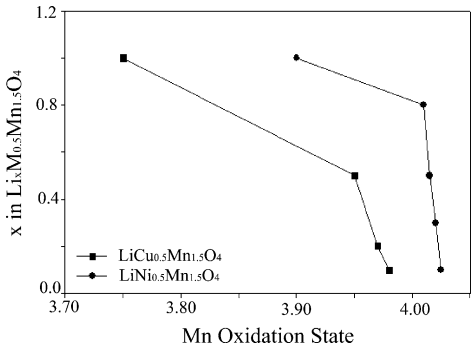

Fig. 3. Oxidation states of Mn as a function of second divalent metal substitution in $LiNi_{0.5}Mn_{1.5}O_4$ and $LiCu_{0.5}Mn_{1.5}O_4$ as determined from in situ XANES spectroscopy in their second charge profile.

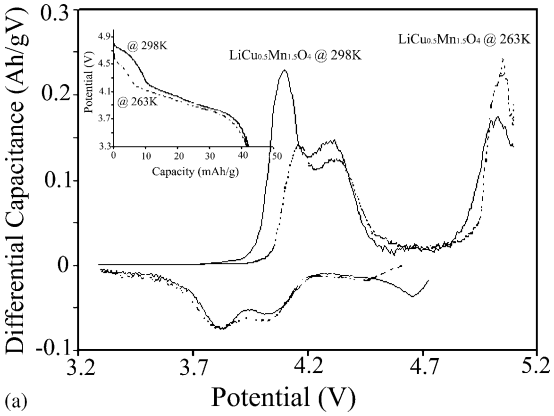

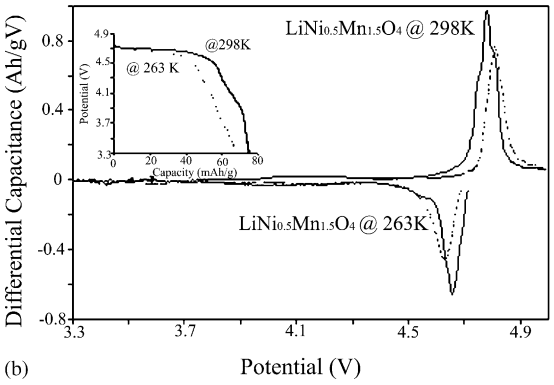

Fig. 4. Differential capacitance profile for: (a) $LiCu_{0.5}Mn_{1.5}O_4$ cycled at 298 K (—) and 263 K (- - -). Corresponding discharge profiles at 298 K (—) and 263 K (- - -) is shown in the inset and (b) $LiNi_{0.5}Mn_{1.5}O_4$ cycled once at 298 K (—) and 263 K (- - -). Corresponding discharge profiles at 298 K (—) and 263 K (- - -) is shown in the inset. Charge/discharge rate was *C*/10 in all experiments.

The major reason for the different oxidation states of Mn relates to the rearrangement of the divalent ion in the spinel matrix;

(i) copper resides both at the Li *A* sites and the Mn *B* sites (in the AB_2O_4 spinel structure) while,
(ii) Ni is incorporated in the spinel matrix, especially into the manganese *B* site (in the AB_2O_4 spinel structure) in higher concentration as compared to copper inclusion [12].

Therefore, it is expected that these materials would not be subjected to JT distortions even at reduced temperatures, as can be seen in Fig. 4a and b. Although no change in the discharge capacities is detected, a marked change in differential capacitance profile is observed for both $LiCu_{0.5}Mn_{1.5}O_4$ and $LiNi_{0.5}Mn_{1.5}O_4$ as a function of temperature. Fig. 4a presents the electrochemical behavior of Cu-doped manganese spinel. The first set of peaks of the Ox–Red system at ∼4 V, (which are representative of the two-phase transformation attributed to Mn oxidation and reduction, respectively) [7] is shifted by approximately 100 mV to a higher potential. The third reversible Ox–Red peak position at ∼5 V, attributed to the reversible oxidation of copper(II) to copper(III) [10–13], is unchanged. Fig. 4b presents the electrochemical behavior of Ni-doped manganese spinel. The oxidation and reduction processes of this material are dominated by the Red–Ox reaction of nickel (Ni(II) to Ni(IV)) [23], in agreement with the changes in the Mn oxidation states (Fig. 3). Thus, the capacity obtained from reactions associated with manganese Red–Ox is minor compared with the overall capacity of the Ni-doped spinel material. The electrochemical charging of Cu-doped spinel at low temperature causes the 4 V peak to be shifted to a higher potential (by approximately 100 mV) with a concomitant reduction in the capacity associated with the Mn oxidation state change (observed both in the differential capacity curve and as well in the charge profile), while the peak positioned at the higher potential (4.9 V) remains intact. In the case of the Ni-doped spinel, no change in either capacity or a significant shift in potential was observed (Fig. 4b). However, a significant alteration between the two materials is observed upon discharging. Ni-modified manganese spinel cathode material exhibited almost no change in the potential or discharge capacity in the 4.6 V plateau at 263 K (Fig. 4b), while Cu-modified manganese spinel suffers from the exposure to a low temperature and exhibits almost no discharge capacity (Li-ion intercalation into the solid matrix) at the high-potential (Fig. 4a) plateau. The lower potential twin peaks associated with Mn reduction (3.9–3.8 V) remains intact. At this stage of the research we can only assume that this significant difference in the observed behavior is related to the crystallographic difference between the two materials, namely the evolution and co-existence of several cubic phases in the charge/discharge profile of the Ni-modified manganese spinel versus a single cubic phase for the Cu-doped analog [13].

Another route to increase the oxidation state of manganese is by producing Li-rich materials of the type $Li(Li_xMn_{2-x})O_4$. The oxidation state of manganese can be increased from 3.5 up to 4, depending on the degree and level of lithium substitution into the manganese 16d sites. As discussed earlier, Yamada [1] demonstrated that upon increment of x from 0 to 0.039 in $Li(Li_xMn_{2-x})O_4$, the transition temperature (from cubic into tetragonal phase) decreases until the transition is no longer observed by DSC beyond $x = 0.033$.

Fig. 5 presents differential capacitance profile of $LiMn_2O_4$ cycled at 298 K. A two-phase transition process is observed in the 4 V region, indicated by the appearance of twin Red–Ox peaks (4.1 and 4.2 V (Ox); 4.1 and 3.9 V (Red)). Identification of the two distinct phases is highly difficult once $LiMn_2O_4$ is being cycled at 263 K, as the two peaks became essentially a single oxidation peak. In addition, the charge (capacity = area under the peak) was greatly reduced relative to the charge (combined peak area) associated with the process at 298 K, which is further exemplified by the discharge capacity (Fig. 5 inset). The position of the peak at 263 K was also effected by the charge and discharge rate. At a *C*/10 rate, the peak was situated at 4.28 V (Ox) and 3.9 V (Red), while lowering the charge/discharge rate to *C*/20 sit-

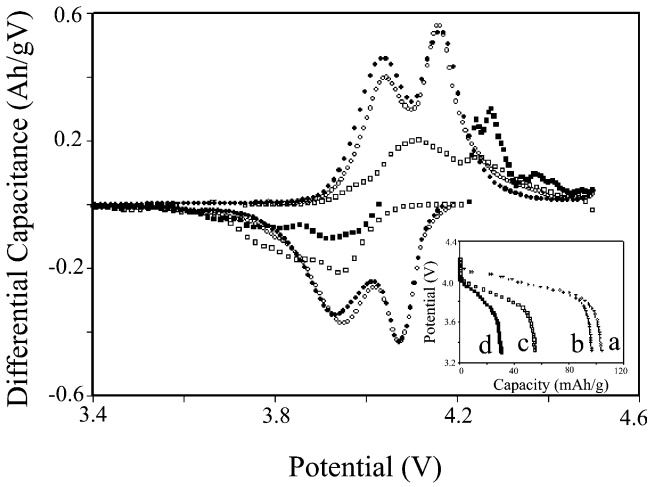

Fig. 5. A comparison of differential capacitance profiles of $LiMn_2O_4$ cycled at four different conditions; (●) cycled at 298 K at C/10; (■) cycled at 263 K at C/10 rate; (○) cycled at 298 K after 263 K cycling; (□) cycled at 263 K at C/20 rate. Inset: a comparison of discharge profiles of $LiMn_2O_4$ cycled at four different conditions: (a) cycled at 298 K at C/10 rate; (b) cycled at 263 K at C/10 rate; (c) cycled at 298 K after 263 K cycling; (d) cycled at 263 K at C/20 rate.

uated the peak at 4.1 V (Ox) and 3.9 V (Red). The positive shift observed at low temperature could be attributed to either a pronounce decrease in electrolyte conductivity at this temperature [27–29] and/or an increase in the electrode solid resistivity [4,5].

It is our understanding that the effect of electrolyte conductivity should not be considered as the prime cause explaining this behavior, since the peak position at the 5 V region for the copper and Ni-doped systems observed during the charging step (Fig. 4a and b) was not effected. Thus, the observed performance of $LiMn_2O_4$ at 263 K is suggested to be due to thermally induced structural changes, leading to modification in the material electrochemical behavior.

The observed reduced capacity at 263 K is maintained over the whole cycle life. Both the capacity and the differential capacitance profiles obtained from $LiMn_2O_4$ cathode materials are fully recovered once the cell is cycled back at 298 K, subsequent to cycling at 263 K. Capacity fading was not apparent at either operating temperature over the evaluated cycle life and repeated switching between temperature conditions. The presence of only one Ox–Red peak at operating conditions of 263 K would suggest some loss of lithium ordering in the spinel matrix, which is observed not only electrochemically (differential capacitance profiles), but also by in situ XRD studies [17,25,26].

Rodriguez-Carvajal et al. [30] and Rousse et al. [2] observed a slow pseudo-orthorhombic transition of $LiMn_2O_4$. They also suggested five crystallographic sites in which Mn^{3+} and Mn^{4+} are located. Two of these sites occupy hole-rich Mn^{4+} [Mn(IV) and Mn(V)] and the other three are occupied by electron rich Mn^{3+} [Mn(I), Mn(II) and Mn(III)]. This arrangement of charges forbids the hopping of electrons, which would be consistent with the concept of discreet energy bands, being formed as a result of JT distortion. This results in charge localizing and disrupting hopping mechanism for charge conduction.

We consider the initial loss in capacity as being originated from Mn^{3+} and Li^+ ions interactions during the pseudo-orthorhombic distortion. The electrostatic interaction of these two species is the result of the accompanying electron (that would be associated with the transfer of lithium ion in and out of the lattice), being localized due to the loss of a conduction pathway. Upon charging the material, we observe that the triplet splitting of the (3 1 1) peak reverts back to a single peak (Fig. 2b). These structural changes can be detected in the differential capacitance profiles, as well. Note that even with the reduced amount of lithium moving in and out of the solid matrix, we observe in a slight retention of the two peaks in the 4 V region (not easily resolved). The significant difference between the results obtained at low temperature and the results obtained at 298 K is that the 'valley' between the two peaks is almost lost. This may indicate a loss of lithium ion ordered state in the solid, commonly associated with $Li_{0.5}Mn_2O_4$.

4. Conclusions

The data presented in this report shows that structural changes resulting from cycling $LiMn_2O_4$ at low temperatures are originated from the existence of mixed cubic and tetragonal phases. The observed reduced capacity is attributed to Mn^{3+} and Li^+ ions static interactions. Partial capacity recovery is possible at temperatures below the transition temperature, as the number of Mn^{3+} and Li^+ ions static interactions is minimized. Structural, and hence the capacity recovery of the cubic phase, are all fully reversible once the material temperature is raised, back from 263 K and cycled at 298 K. Capacity fading is never observed at 263 K despite the increased Mn^{3+}/Mn^{4+} ratio. Thus, the disproportionate reaction is not relevant at reduced temperatures. The explanation for this is that the thermally-induced JT distortion is being achieved through the bulk of the material, alleviating structural stress and strain. However, once the Mn^{3+}/Mn^{4+} ratio is increased by the insertion of excess Li-ions, the structural changes induced by the JT active Mn^{3+} species is surface propagated, resulting in non-uniform structural stress of the spinel structure, thus, degradation and capacity fading occur. This work has shed some light into structural distortion and on the performance of $LiMn_2O_4$ cycled at low temperatures. More work (in situ XRD) is scheduled aiming in understanding the low temperature behavior of modified manganese spinels.

Acknowledgements

The authors wish to acknowledge the financial support from Northeastern University (start up grant), the Research

and Development Foundation at the Technion-Israel Institute of Technology and the US Department of Energy (Cooperative Research and Development Agreement, CRADA). The authors also gratefully acknowledge the financial support from the US Department of Energy, Division of Materials Science for its role in the development and operation of beam line X11A and X18A at the NSLS under contract number DE-FG05-89ER45384. The NSLS is supported by the Department of Energy, Division of Material Science under contract number DE-AC02-98CH 10886.

References

[1] A. Yamada, M. Tanaka, Mater. Res. Bull. 30 (1995) 715.
[2] G. Rousse, C. Masquelier, J. Rodriguez-Carvajal, M. Hervieu, Electrochem. Solid-State Lett. 2 (1999) 6.
[3] V. Massarotti, D. Capsoni, M. Bini, G. Chiodelli, J. Solid State Chem. 131 (1997) 94.
[4] J. Molenda, K. Swierczek, W. Kucza, J. Marzec, A. Stoklosa, Solid State Ionics 123 (1999) 155.
[5] Y. Shimakawa, T. Numata, J. Tabuchi, J. Solid State Chem. 131 (1997) 138.
[6] M. Atanasov, J.-L. Barras, L. Benco, C. Daul, J. Am. Chem. Soc. 122 (2000) 4718.
[7] G. Amatucci, J.-M. Tarascon, J. Electrochem. Soc. 149 (2002) 31.
[8] J.M. Tarascon, E. Wang, F.K. Shokoohi, W.R. McKinnon, S. Colson, J. Electrochem. Soc. 138 (1991) 2859.
[9] Y. Xia, M. Yoshio, J. Power Sources 66 (1997) 129.
[10] Y. Ein-Eli, W.F. Howard, J. Electrochem. Soc. 144 (1997) L205.
[11] Y. Ein-Eli, W.F. Howard Jr., S.H. Lu, S. Mukerjee, J. McBreen, J.T. Vaughey, M.M. Thackeray, J. Electrochem. Soc. 145 (1998) 1238.
[12] Y. Ein-Eli, S.H. Lu, S. Mukerjee, J. McBreen, J. Electrochem. Soc. 145 (1998) 3383.
[13] Y. Ein-Eli, S. Mukerjee, X.Q. Yang, J. McBreen, J.T. Vaughey, M.M. Thackerey, J. Electrochem. Soc. 146 (1999) 908.
[14] S. Mukerjee, X.Q. Yang, X. Sun, S.J. Lee, J. McBreen, Y. Ein-Eli, Electrochim. Acta 49 (2004) 3373.
[15] J. McBreen, S. Mukerjee, X.Q. Yang, T.R. Thurston, N.M. Jisrawi, in: O'Savadoga, F. Roberge (Eds.), Proceedings of the 2nd International Symposium on New Materials for Fuel Cells and Modern Battery Systems, July 6–10, 1997.
[16] X.Q. Yang, X. Sun, S.T. Lee, S. Mukerjee, J. McBreen, Electrochem. Solid-State Lett. 2 (1999) 157.
[17] S. Mukerjee, T.R. Thurston, N.M. Jisrawi, X.Q. Yang, J. McBreen, J. Electrochem. Soc. 145 (1998) 466.
[18] S. Mukerjee, X.Q. Yang, X. Sun, S. Lee, J. McBreen, Y. Ein-Eli, Electrochim. Acta 49 (2004) 3373.
[19] X.Q. Yang, X. Sun, M. Balasubramanian, J. McBreen, Y. Xia, T. Sakai, M. Yoshio, Electrochem. Solid-State Lett. 4 (2001) A117.
[20] H. Hiroshi, T. Toshimi, E. Hirotoshi, A. Etsu, J. Mater. Sci. Lett. 17 (1998) 811.
[21] T. Izumi, K. Yusuke, T. Yorihiko, Phys. Rev. B 64 (2001) 094422/1.
[22] A. Yamada, J. Solid State Chem. 122 (1996) 160.
[23] Y. Gao, K. Myrtle, M. Zhang, J.N. Reimers, J.R. Dahn, Phys. Rev. B 54 (1996) 3878.
[24] Q. Zheng, A. Bonakdarpour, M. Zhang, Y. Gao, J.R. Dahn, J. Electrochem. Soc. 144 (1997) 205.
[25] W. Liu, K. Kowal, G.C. Farrington, J. Electrochem. Soc. 145 (1998) 459.
[26] Y.J. Lee, F. Wang, S. Mukerjee, J. McBreen, C.P. Gray, J. Electrochem. Soc. 147 (2000) 803.
[27] Y. Ein-Eli, S.R. Thomas, R. Chadha, T.J. Blakely, V.R. Koch, J. Electrochem. Soc. 144 (1997) 823.
[28] Y. Ein-Eli, S.F. McDevitt, R. Laura, J. Electrochem. Soc. 145 (1998) L1.
[29] H.-C. Shiao, D. Chua, H.-P. Lin, S. Slane, M. Salomon, J. Power Sources 87 (1–2) (2000) 167.
[30] J. Rodriguez-Carvajal, G. Rousse, C. Masquelier, M. Hervieu, Phys. Rev. Lett. 81 (1998) 4660.